crystals

MDPI

Article

# Analysis of the Effect of Copper Doping on the Optoelectronic Properties of Indium Oxide Thin Films and the Thermoelectric Properties of an $In_2O_3$/Pt Thermocouple

**Yantao Liu *, Tao Lin *, Rong Huang *, Jiahao Shi and Sui Chen**

Department of Electronic Engineering, Xi'an University of Technology, Xi'an 710048, China; 2210321284@stu.xaut.edu.cn (J.S.); 2210321265@stu.xaut.edu.cn (S.C.)
* Correspondence: liuyt@xaut.edu.cn (Y.L.); lintao@xaut.edu.cn (T.L.); 2210320014@stu.xaut.edu.cn (R.H.)

**Abstract:** The detection and real-time monitoring of temperature parameters are important, and indium oxide-based thin film thermocouples can be integrated on the surface of heaters because they operate normally under harsh conditions and provide accurate online temperature monitoring. The higher stability and appropriate optical and electrical properties of $In_2O_3$ make it very suitable as an electrode material for thermocouple sensors. This work demonstrates that copper doping can alter the optical and electrical properties of $In_2O_3$ films and regulate the output performance of thermocouples. Copper-doped $In_2O_3$ thin films were prepared using the magnetron co-sputtering method. The doping concentration of Cu was controlled using direct current (DC) power. An $In_2O_3$/Pt thermocouple sensor was prepared, and the optoelectronic and thermocouple properties were adjusted by changing the copper doping content. The thickness valve of the thin film sample was 300 nm. The results of the X-ray diffraction suggested that the structure of the doped $In_2O_3$ thin films was cubic. The results of the energy-dispersive X-ray analysis revealed that Cu was doped into the $In_2O_3$ thin films. All deposited films were n-type semiconductor materials according to Hall effect testing. The 4.09 at% Cu-doped thin films possessed the highest resistivity ($30.2 \times 10^{-3}$ Ω·cm), a larger carrier concentration ($3.72 \times 10^{20}$ $cm^{-3}$), and the lowest carrier mobility (0.56 $cm^2V^{-1}s^{-1}$). The optical band gap decreased from 3.76 to 2.71 eV with an increase in the doping concentration, and the transmittance of the film significantly reduced. When the DC power was increased, the variation range of Seebeck coefficient for the $In_2O_3$/Pt thermocouple was 152.1–170.5 μV/°C, and the range of thermal output value was 91.4–102.4 mV.

**Keywords:** $In_2O_3$ thin film; Seebeck coefficient; transmittance; thermocouple

check for updates

**Citation:** Liu, Y.; Lin, T.; Huang, R.; Shi, J.; Chen, S. Analysis of the Effect of Copper Doping on the Optoelectronic Properties of Indium Oxide Thin Films and the Thermoelectric Properties of an $In_2O_3$/Pt Thermocouple. *Crystals* **2024**, *14*, 78. https://doi.org/10.3390/cryst14010078

Academic Editor: Andrei Vladimirovich Shevelkov

Received: 27 December 2023
Revised: 9 January 2024
Accepted: 11 January 2024
Published: 13 January 2024



## 1. Introduction

Transparent conductive oxide (TCO) thin films have a significant research value and are widely used in many applications such as solar cells, display devices, photoelectronic devices, and touchscreens [1–4]. Metal oxides commonly used in TCO thin film systems include cadmium oxide (CdO), zinc oxide (ZnO), tin oxide ($SnO_2$), and indium oxide ($In_2O_3$) [5–8]. The demand for TCO thin films has increased over the last few years with the rapid development of various devices. $In_2O_3$ is an n-type semiconductor. Its band gap is 3.5–3.7 eV, and it is widely used in transparent conducting electrodes, solar cells, displays, and photoelectric sensors [9,10].

The electrical and optical properties of an $In_2O_3$ thin film can be improved by doping metal elements such as Sn, Cr, Mo, Ce, Sb, Li, Zn, and Cu [11–22]. Pramod et al. prepared Sb-doped $In_2O_3$ films [18]; the highest optical transmittance was obtained at 1.5 at.%, and the doping amount was able to change the optical band gap of the $In_2O_3$ films. Ahmed et al. prepared $(In_{1-x}Cr_x)_2O_3$ thin films under different Cr doping concentrations [16]. As the Cr doping concentration increased, the films preferentially oriented along the (222) direction under different component conditions, and the optical band gap value increased from

3.21 eV to 3.46 eV. Shi et al. prepared Ce-doped $In_2O_3$ thin films under low-temperature conditions using radio frequency reactions [17]. According to an electrical performance test, the carrier concentration of the films reached $2.1 \times 10^{20}$ $cm^{-3}$, and the highest mobility obtained was 153.7 $cm^2/Vs$. Wang et al. prepared $In_2O_3$ thin films with a resistivity of $3.76 \times 10^{-4}$ Ω·cm by doping Hf [18]. Their study revealed that the Hall mobility could reach 79.6 $cm^2/Vs$, and the average transmittance of the thin film could reach 83% in the range of 300–1500 nm. Indium–gallium–zinc oxide (IGTO) thin films on flexible substrates were developed by Kang et al. using co-doping with Ga and Ti when the oxygen flow was zero [19]. The sheet resistance of IGTO was 39.3 Ω/sq, and the transmittance of the IGTO film reached 86.96%. Kaleemulla et al. prepared Mo-doped $In_2O_3$ thin films on glass substrates using the activated reactive evaporation method [20]. The films synthesized at a Mo doping level of 3% and a substrate temperature of 573 K. The electrical resistivity achieved a minimum value of $5.2 \times 10^{-4}$ Ω·cm, the average optical transmittance of the films reached 90%, and the band gap was 3.68 eV. Fan Ye et al. prepared Cu-doped $In_2O_3$ using the reactive DC magnetron sputtering method [21]. The results revealed that Cu doping could significantly alter the electrical and optical properties of thin films. The resistivity of the doped $In_2O_3$ thin films reached 1.82 Ω·cm, and the minimum optical band gap could be reduced to 3.70 eV. Otto J. Gregory constructed Cu-In-O thin films [22], and found that in a composition of 40.0 atom % indium, thin films can transition from p-type to n-type conduction.

The common methods used In the preparation of $In_2O_3$ thin films include sol–gel, pulsed laser deposition (PLD), metal–organic chemical vapor deposition (MOCVD), and magnetron sputtering [23–28]. Gupta et al. prepared Gd-doped $In_2O_3$ films on quartz substrates using the PLD method [23]. Under a vacuum and 600 °C growth conditions, high-conductivity indium oxide thin films were obtained with a carrier concentration of $1.74 \times 10^{20}$ $cm^{-3}$, a resistivity of $2.80 \times 10^{-4}$ Ω·cm, and a mobility of $1.28 \times 10^2$ $cm^2V^{-1}s^{-1}$. Sanchez et al. prepared $In_2O_3$ thin films on the c-axis of sapphire substrates using a low-temperature sol–gel method [24]. They observed an increase in the carrier concentration of the films to $2.45 \times 10^{19}$ $cm^{-3}$, with a resistivity of 3.5 Ω·cm noted after heat treatment at 700 °C. Baqiah et al. prepared $In_2O_3$ thin films using the CVD method, with $InCl_3 \cdot 4H_2O$ as the initial raw material [25]. The resistivity of the films in their study reached $1.458 \times 10^{-2}$ V·cm at a deposition temperature of 720 K. According to Du et al., the resistivity of $In_2O_3$ thin films prepared using the MOCVD method could reach $1.458 \times 10^{-2}$ V·cm at a deposition temperature of 720 K [26]. Compared with other preparation methods, the magnetron sputtering method is widely used in certain areas because of its superiority in terms of uniformly deposited films, its high purity, and wide application to target materials. Cho used a radio frequency reaction method to prepare $In_2O_3$ thin films on target materials [27]. The films were preferentially oriented along the (222) and (400) directions, and the average transmittance reached 88.6% in the range of 370–1100 nm. Yuan et al. prepared $In_2O_3$ thin films on amorphous glass using the magnetron sputtering method [28]. A high field-effect mobility of thin film transistors was obtained by optimizing the annealing process.

Due to its excellent stability and significant thermoelectric potential output under high-temperature conditions, indium oxide is often used as an electrode material for high-temperature thermocouples [29–31]. Its thermoelectric output characteristics can be adjusted via doping with indium oxide thin films. Liu Dan et al. prepared indium oxide thin films using radio-frequency magnetron sputtering, and constructed $La_{0.8}Sr_{0.2}CrO_3/In_2O_3$ thermocouples [32]. The thermoelectric potential output reached 305.8 μV/°C at 1100 °C. By doping Sn to adjust the thermoelectric output characteristics of indium oxide thin films, Xiaohui Zhao et al. used magnetron sputtering to construct ITO/Pt thin film thermocouples on nickel alloy substrates. A high-temperature tolerance of up to 1100 °C was recorded [33]. To improve the stability of thermocouples, Zhongkai Zhang et al. constructed $In_{1.35}ZnO_{2.11}/In_2O_3$ thermocouples using screen-printing technology. This resulted in a thermoelectric potential output of 39.8 μV/°C at 1500 °C. The drift rate was 0.84 °C/h [34].

Zhao X.H et al. prepared ITON-InON ceramic thin film thermocouples [35]; the samples were heated at 1000 °C for 5 h in a nitrogen-rich atmosphere and 5 h in air, respectively, which improved the output stability of the thermocouple, and the average Seebeck reached 64.7 μV/°C. Liu et al. treated indium oxide thin films at a high temperature of 1150 °C for 10 h, and the $In_2O_3$/ITO thermocouple was able to output normally [36].

In this study, we prepared copper-doped thin films using the co-sputtering method, achieved indium oxide thin films with adjustable transmittance and electrical properties, and obtained thin film thermocouples with an adjustable output thermal voltage. We investigated the electrical and optical properties of undoped $In_2O_3$ and Cu-doped $In_2O_3$ thin films, the effect of the Cu ion concentration on the microstructure, and the electrical and optical properties of $In_2O_3$. The thermoelectric properties of the $In_2O_3$/Pt thermocouple were systematically characterized.

## 2. Materials and Methods

$In_2O_3$ was created on quartz substrates with different concentrations of copper doping using magnetron co-sputtering equipment (SP3-80C, Chuangshiweina Technology Co., Beijing China). We altered the direct current (DC) sputtering power during the preparation process to obtain the different Cu-doping concentrations. The samples of $In_2O_3$ with different Cu-doping concentrations (sputtered by DC power) were prepared at room temperature using DC sputtering power supplies of 10 W, 15 W, 20 W, and 25 W. The diameter of all $In_2O_3$ and Cu targets was 80 mm, and the purity of both the $In_2O_3$ and Cu targets was 99.99%. The $In_2O_3$ target was set at a sputtering power of 100 W using a radio-frequency power supply throughout the entire sputtering process. Before sputtering, substrates with a size of 10 mm × 10 mm and a thickness of 0.7 mm were cleaned for 15 min in an ultrasonic bath using alcohol and acetone separately. These were then repeatedly rinsed using deionized water and dried with a high-pressure nitrogen gun. The base pressure of the chamber was $6.0 \times 10^{-4}$ Pa, and the sputtering pressure was 1.5 Pa. The substrates were rotated at 14 revolutions per minute (rpm) during the deposition process. The oxygen-to-argon ratio was set at 1:6, the argon gas flow rate was maintained at 60 standard cubic centimeters per minute (sccm), and the sputtering time was set at 3 h. After the sputtering process, the thin films were annealed in a high-temperature atmosphere furnace (OTF-1200X; MTI, Hefei, China) at 500 °C in an air atmosphere for 1 h. The parameters of the indium oxide and copper targets during co-sputtering are presented in Table 1, and the magnetron co-sputtering of $In_2O_3$ doped with Cu is diagrammatically represented in Figure 1.

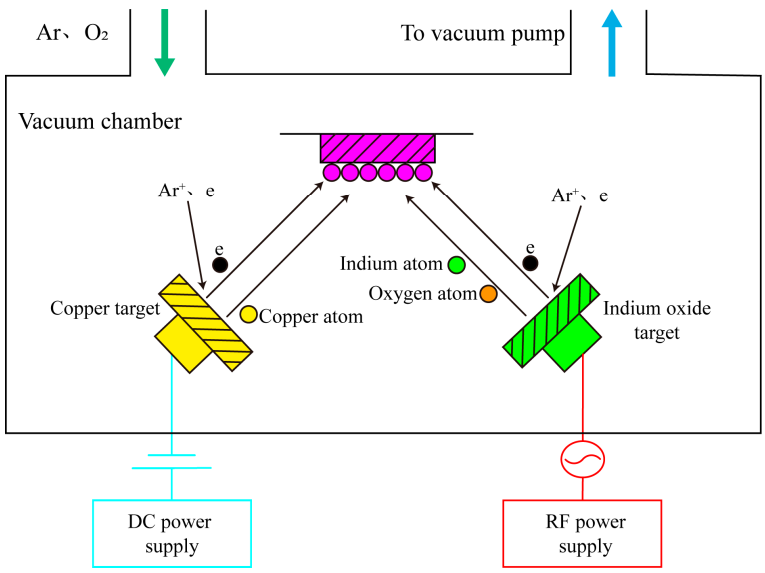


**Figure 1.** Schematic diagram of magnetron co-sputtering.

**Table 1.** Parameters of indium oxide and copper targets during co-sputtering.

| Target | Sputtering Method | Sputtering Power (W) | Sputtering Time (h) | Argon Gas Flow Rate (sccm) | Oxygen Flow Rate (sccm) |
|---|---|---|---|---|---|
| $In_2O_3$ | RF | 100 | 3 | 60 | 10 |
| Cu | DC | 0–25 | 3 | | |

The pure and doped $In_2O_3$ thin films were tested using an X-ray diffractometer (XRD) (Ultima IV, Rigaku, Hitachi, Tokyo, Japan). The surface images and EDX patterns of the thin film samples were determined using an SEM (Quanta 250, FEI, Hillsboro, OR, USA) equipped with an energy-dispersive spectrometer. The surface topography of the thin films was characterized by an AFM (Dimension Icon, Bruker, Billerica, MA, USA). The electrical and optical properties of the $In_2O_3$ thin films were investigated using a Hall effect testing system (CH300, CH-Magnetoelectricity Technology, Beijing, China) and an ultraviolet-visible spectrophotometer (Lamda950, PerkinElmer, Waltham, MA, USA), respectively.

To obtain the Seebeck coefficient of the pure and doped $In_2O_3$/Pt thermocouples, all of the films were fabricated (Figure 2). The length, width, and thickness of the quartz substrate were 10 cm, 10 mm, and 1.5 mm, respectively. After the deposition of $In_2O_3$ and Pt thin films, an $In_2O_3$ thin film with a width of 2.5 mm and a length of 9.5 cm was obtained. The Pt electrode was 2.5 mm, with a length of 9.5 cm. The overlapping area of the two electrodes was 2.5 mm × 2.5 mm. The preparation process is presented in Figure 3. First, pure and Cu-doped $In_2O_3$ thin films were fabricated using the co-sputtering method and a stainless steel metal mask to form an indium oxide electrode pattern. Second, the pure and Cu-doped $In_2O_3$ thin films were annealed in an air atmosphere at 500 °C for 1 h. Third, the Pt electrode was obtained using a sputtering system (JPG560, SKY Technology Development Co., Ltd., China) and a metal mask to form a Pt electrode pattern. The hot-end overlap area was 2.5 mm × 2.5 mm. The Pt target had a diameter of 4 inches, and the thickness was 4 mm. The instrumental settings of the sputtering process during the formation of the Pt electrode were a sputtering pressure of 0.5 Pa, a sputtering power of 100 W, and an argon flow rate of 80 sccm. The thickness of the obtained Pt thin film was approximately 300 nm.

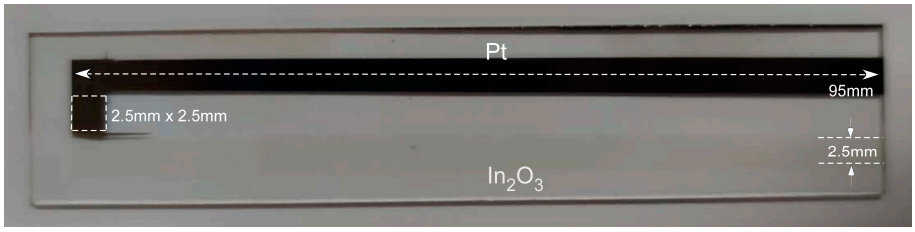


**Figure 2.** Physical image of a test sample of an $In_2O_3$/Pt thermocouple.

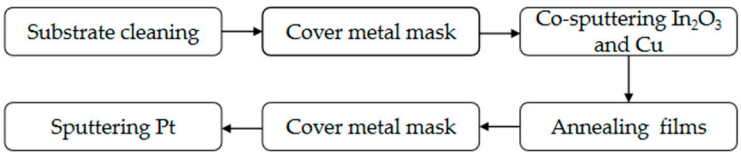


**Figure 3.** The process diagram of the $In_2O_3$/Pt thermocouple preparation.

As presented in Figure 4, the Seebeck coefficient and thermal voltage test system mainly consisted of one heating furnace, one voltmeter, two thermometers, and one cooling plate. A Nabertherm high-temperature heating furnace (LHT 2-17, Nabertherm, Lilienthal, Germany) was adapted to heat the hot end of the sample. The measurement range was set from room temperature to 600 °C, and the length of the K-type thermocouple was 20 cm. This was inserted into the high-temperature furnace to test the temperature of the hot end

of the sample. Alumina foam transfer and high-temperature asbestos material were used between the hot and cold ends to insulate the treatment. The hot end of the film sample was pushed into the heating furnace to obtain the high-temperature difference between the two ends. An alumina foam brick was used as insulation material for the furnace door. A voltmeter was used to measure the output voltage of the cold end. Standard *K*-type thermocouples were used to measure the temperature of the hot and cold ends. The cold end was cooled by circulating water throughout the whole process, and the voltmeter was used to display the value of the thermal voltage.

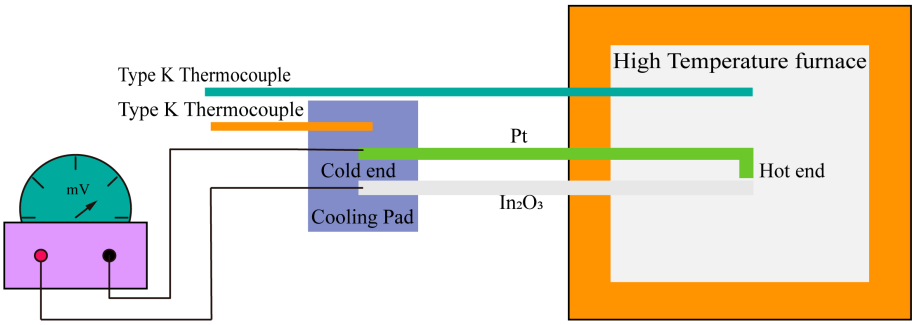


**Figure 4.** Schematic diagram of the thermal voltage testing system.

## 3. Results

### *3.1. Microstructure and Other Physical Characteristics of Cu-Doped $In_2O_3$ Thin Films*

The phase structure of the prepared thin film samples was determined using the XRD patterns obtained from 25° to 65°, with a 0.15418 nm wavelength of Cu K-alpha radiation. As demonstrated in Figure 5a, the cubic phase of $In_2O_3$ was observed in all thin film samples, and the space group was $Ia\bar{3}$. No other peaks were observed, which implied that Cu doping had not added impurities, and that Cu was well incorporated into the lattice of the cubic $In_2O_3$ and had replaced the In atom. However, two new crystal phases with peaks of (431) and (611) simultaneously appeared. Figure 5b demonstrates the gradual shift in the peak (622) orientation of the doped thin film sample with an increase in the doping concentration. A similar observation was reported by Ye et al. [21]. The atomic radius of Cu is smaller than that of an In crystal; the substitution of smaller Cu for larger In could have changed the phase structure of the crystal, thereby shifting the corresponding diffraction peaks [37].

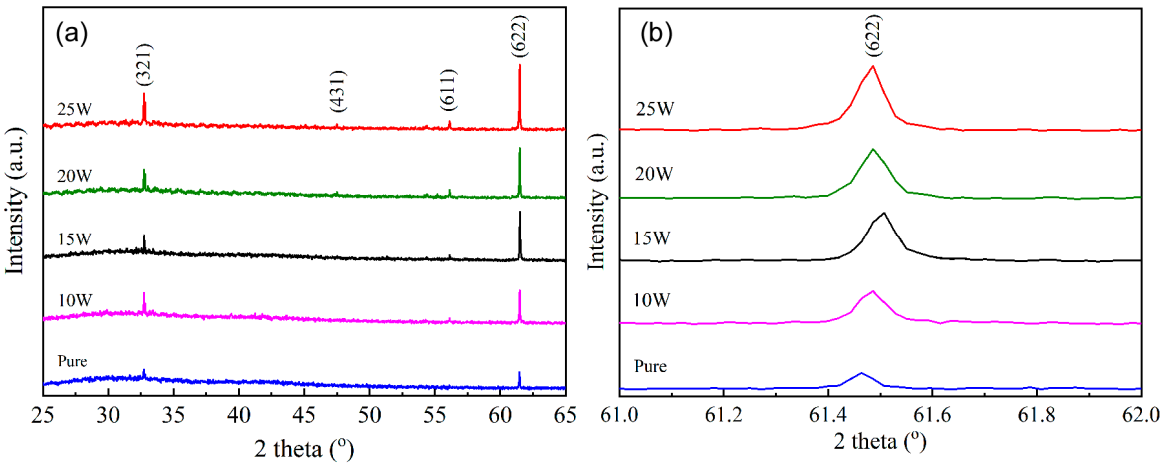


**Figure 5.** (**a**) XRD patterns of Cu-doped thin film samples; (**b**) diffraction peaks (622).

Figure 6 presents the crystal size values of the Cu-doped $In_2O_3$ films obtained using different DC sputtering powers. The grain size was estimated according to the Scherrer formula [38] (Equation (1)):

$$D = 0.9\lambda / \beta \cos\theta \quad (1)$$

where $\lambda$ is the X-ray wavelength, $\theta$ is the Bragg diffraction angle, and $\beta$ is the full width at half maximum of the (622) peak. The increase in the DC sputtering power increased the full width at half maximum (FWHM) of the Cu-doped $In_2O_3$ films. The size of the crystallite increased from 17.1 nm to 38.9 nm when the DC sputtering power increased from 0 W to 25 W. The maximum value was obtained at DC 25 W. This was mainly attributed to the increase in the sputtering power and the increased number of grain boundary defects.

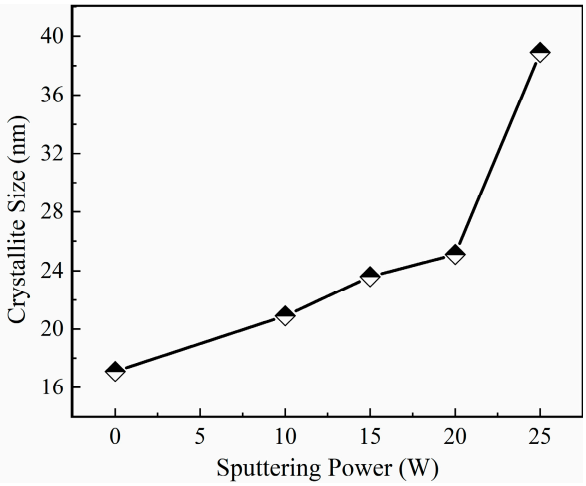


**Figure 6.** Crystallite size of Cu-doped $In_2O_3$ thin films.

Figure 7a shows the the surface topography of unannealed pure film, and Figure 7b–d present the surface topography of the Cu-doped $In_2O_3$ thin film samples under 0 W, 15 W, and 25 W of DC power, respectively. Figure 7b–d reveal that the surface of the film was uniform. A distinct variation in the grain size was absent with an increase in the doping concentration. As presented in Figure 7e, the thickness of the prepared thin film sample was 300 nm. Figure 8 presents the AFM images at different DC sputtering powers; the effects of the Cu-doping concentration on the structural and surface morphology properties of the Cu-doped $In_2O_3$ thin films can clearly be observed. The Cu concentration evidently influenced the surface morphology of the Cu-doped $In_2O_3$ thin films. As the DC sputtering power increased, the grain size increased. This was the same trend of change as calculated from the XRD results. Figure 9 presents the surface roughness. The root mean square (RMS) increased from 4.3 nm to 11.1 nm as the DC sputtering power increased from 0 W to 25 W.

An energy-dispersive X-ray (EDX) analysis was used to further study the element types and contents of the prepared thin films. The EDX patterns of all samples prepared at DC sputtering powers from 0 W to 25 W are presented in Figure 10. The EDX data clearly demonstrate that the Cu doped into $In_2O_3$, and that there was a significant increase in the Cu content with an increase in the sputtering power from 0 W to 25 W. This could be attributed to the participation of Cu in an efficient substitution for indium (In) atoms. The calculated contents of Cu were 1.41%, 1.98%, 4.09%, and 4.26% for the thin film samples prepared at sputtering powers of 10 W, 15 W, 20 W, and 25 W, respectively (Figure 11).

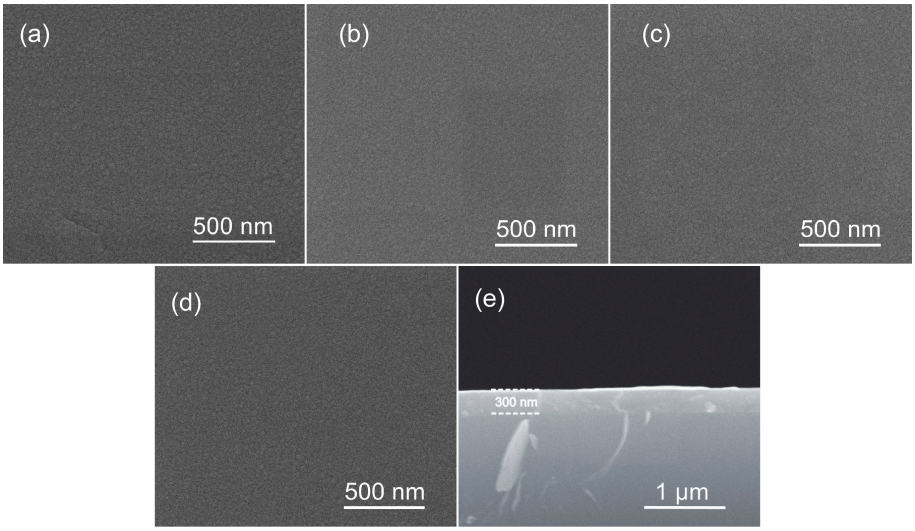


**Figure 7.** Morphology of Cu-doped $In_2O_3$ thin films under different DC powers: (**a**) pure and unannealed; (**b**) 0 W; (**c**) 15 W; (**d**) 25 W. (**e**) Cross-section image under 0 W DC power.

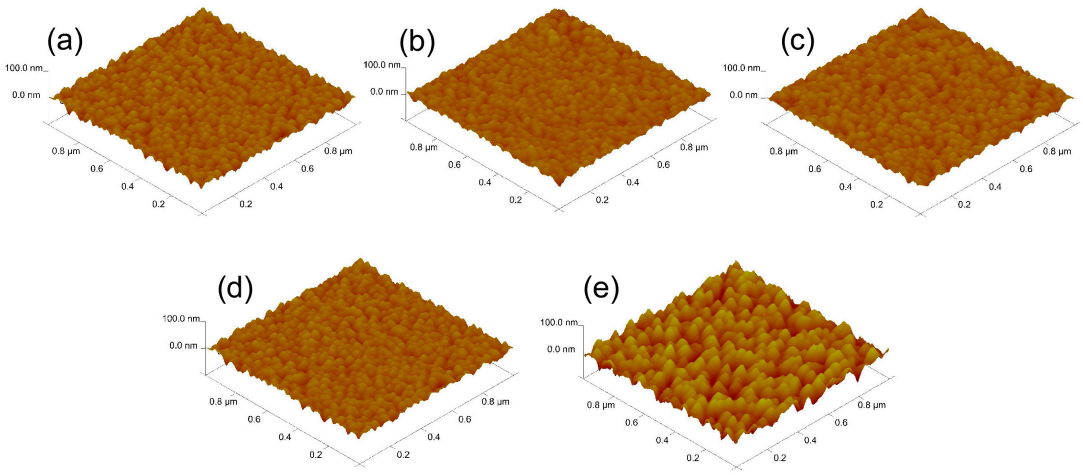


**Figure 8.** AFM images of the surface topography of Cu-doped $In_2O_3$ thin films under different DC powers: (**a**) 0 W; (**b**) 10 W; (**c**) 15 W; (**d**) 20 W; (**e**) 25 W.

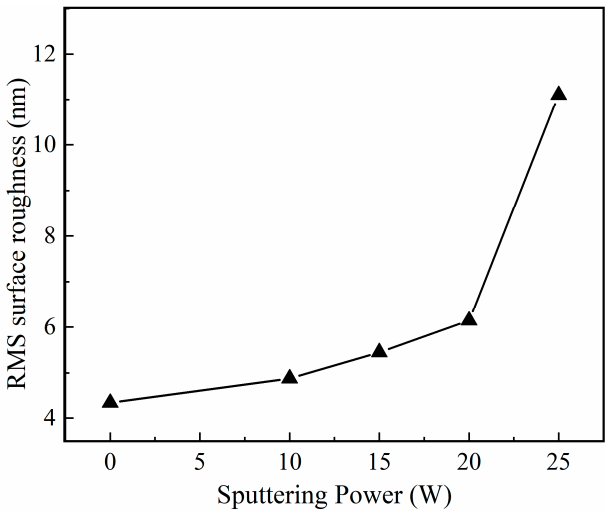


**Figure 9.** Surface roughness of Cu-doped $In_2O_3$ thin films under different DC powers.

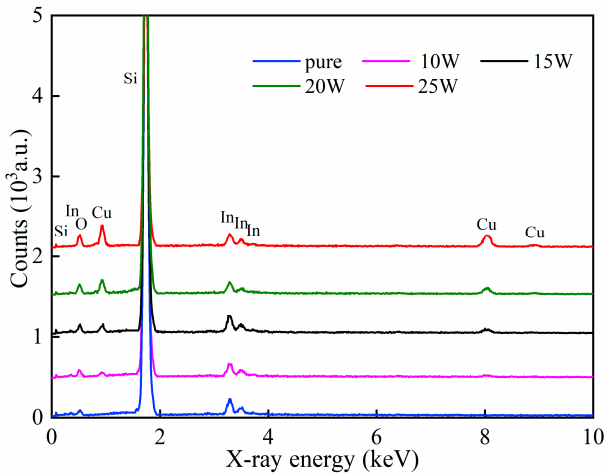


**Figure 10.** EDX patterns of Cu-doped $In_2O_3$ thin films under different DC powers.

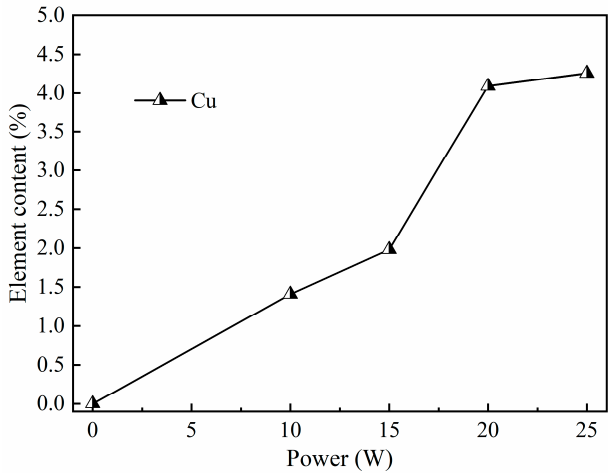


**Figure 11.** Cu content of doped $In_2O_3$ thin films under different DC powers.

### *3.2. Electrical Properties of Cu-Doped $In_2O_3$ Thin Films*

The resistivity ($\rho$), carrier concentration ($n$), and mobility ($\mu$) of all prepared thin film samples were determined using a Hall effect meter at room temperature, and are presented in Figure 12. The Hall effect measurement confirmed that the introduction of Cu did not change the n-type semiconducting behavior of the $In_2O_3$ films. When the sputtering power increased to 15 W, the resistivity also increased from $1.85 \times 10^{-3}$ Ω·cm to $5.17 \times 10^{-3}$ Ω·cm. The carrier concentration remained almost unchanged ($15.3 \times 10^{18}$ $cm^{-3}$) between 0 W and 15 W DC sputtering powers. At a DC sputtering power of 20 W, relatively large changes in resistivity, carrier concentration, and mobility occurred; the values reached were $30.4 \times 10^{-3}$ Ω·cm, $3.72 \times 10^{20}$ $cm^{-3}$, and 0.56 $cm^2V^{-1}s^{-1}$, respectively. The change in the carrier concentration could have occurred for two reasons. It may have been due to the decrease in the band gap of the thin films causing a greater migration of carriers to the conduction band, thereby increasing the carrier concentration. The other reason may have been that the doping of the acceptor Cu could have generated holes to compensate for a negative charge [39,40]. The mobility tended to significantly decrease with an increase in the doping concentration.

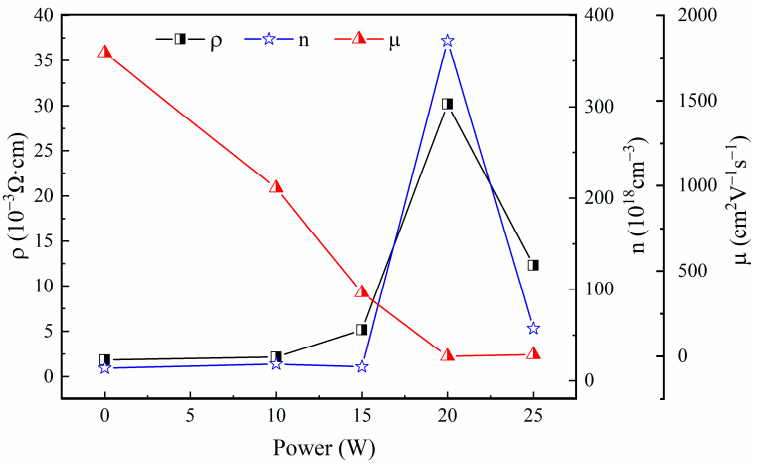


**Figure 12.** Variations in the resistivity, carrier concentration, and mobility of the films under DC sputtering powers.

### *3.3. Optical Properties of Cu-Doped $In_2O_3$ Thin Films*

The transmittance spectra of the Cu-doped $In_2O_3$ films are presented in Figure 13. A clear decrease in transmittance in the visible light region was observed as the Cu sputter power increased from 0 W to 25 W. The average transmittance revealed an overall downward trend. The pure $In_2O_3$ sample was 96% and the doping concentration under 10 W DC power was 85%, whereas the doping concentration decreased to 4.2% under a DC power of 25 W. Consequently, the doping concentration of Cu should not be too high during the preparation of Cu-doped $In_2O_3$ films.

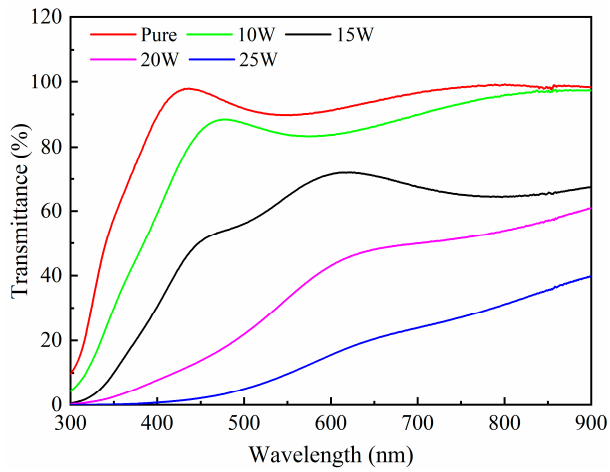


**Figure 13.** Transmittance spectra of $In_2O_3$ thin films.

The optical band gap is an important parameter when studying film properties. The optical band gap of the prepared thin film samples was determined to understand the influence of the doping concentration. The optical band gap was calculated using Equation (2) [41]:

$$(\alpha h\nu)^2 = A(h\nu - E_g) \tag{2}$$

where $h\nu$ is the photon energy. The value of $A$ depends on the direct or indirect band gap. $\alpha$ is the absorption coefficient, which can be determined using a formula that ignores the reflection of light on the film (Equation (3)) [42]:

$$\alpha = \ln\left(\frac{1}{T}\right)/d \tag{3}$$

where $d$ is the thickness of the film (the thickness value was 300 nm) and $T$ is the transmission of the film (as demonstrated in Figure 12). The plot of $(\alpha hv)^2$ vs. $hv$ can then be obtained (as presented in Figure 13) by extending the linear section of the curve to the $x$-axis. The optical band gap can then be determined from the intersection. As presented in Figure 14, the band gap (3.76 eV) obtained for the undoped sample was very close to the values reported in the literature [42] and the doped thin film samples revealed a decrease in the band gap with an increase in the Cu content. Several studies have observed that adding an element to an oxide can narrow the energy band gap of the doped material [43]. Our results also revealed a narrowing of the forbidden band of $In_2O_3$ from doping with Cu.

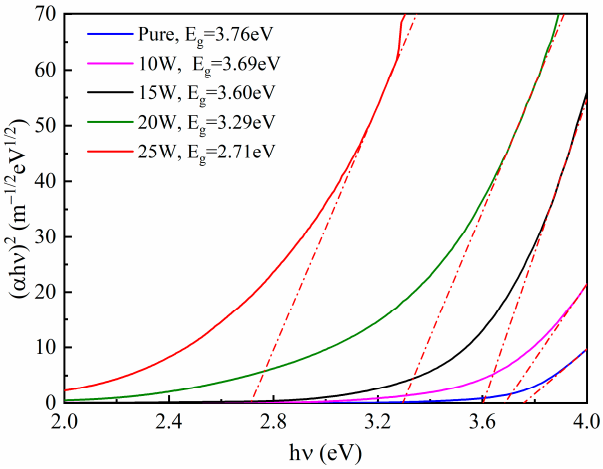


**Figure 14.** $(\alpha hv)^2$ vs. $hv$ of $In_2O_3$ thin films.

### *3.4. Thermoelectrical Properties of Cu-Doped $In_2O_3$ Thin Films*

To measure the output characteristics of the $In_2O_3$/Pt thermocouple, all electrodes were connected using enameled copper wire with a diameter of 0.2 mm and a length of 10 cm. The wire was bonded with silver paste; the contact was between the wire and the two electrodes. Figure 15 presents the thermoelectrical output voltage of the Cu-doped $In_2O_3$ films under different DC powers from room temperature to 600 °C. The output value was 102.4 mV at 0 DC power and a temperature difference of 600 °C. The absolute value of the output thermal voltage of the sample under 20 W DC power was 91.4 mV. The Seebeck coefficients of the Cu-doped $In_2O_3$ thin films were tested as a function of the hot-end temperature. The Seebeck coefficient was obtained using Equation (4) [44]:

$$S = -\frac{\Delta V}{\Delta T} = -(\frac{\Delta V_a - \Delta V_b}{T_h - T_c}) \tag{4}$$

where $S$ is the Seebeck coefficient, $\Delta V$ is the voltage difference between the two different electrode materials, and $\Delta T$ is the temperature difference between the hot end ($T_h$) and the cold end ($T_c$). As $In_2O_3$ is an n-type semiconductor, its output is negative; thus, the absolute value of the Seebeck coefficient of the Pt electrode was much smaller than that of the indium oxide material [45]. Figure 16 presents the trends of the Seebeck coefficient with the temperature variation. The Seebeck coefficient of the Cu-doped $In_2O_3$ films increased with an increase in the temperature difference. When the temperature difference between the two ends of the thin film samples reached 600 °C, the Seebeck coefficient increased to 170.5 μV/°C under 0 DC power. The Seebeck coefficient of Cu-doped $In_2O_3$ thin films under 20 W DC power reached 152.1 μV/°C; it reached 155.6 μV/°C under 25 W DC power. The Seebeck coefficient of the $In_2O_3$ thin films could be expressed by Equation (5) [44]:

$$S(N_D) = -\frac{Ak}{e} - \frac{k}{e}(\frac{(2\pi m_c^* kT)^{\frac{2}{3}}}{h^3 N_D}) \tag{5}$$

where $S$ is the Seebeck coefficient, $k$ is the Boltzmann constant, $e$ is the electron charge, $m_c$ is the effective mass, $h$ is the Planck constant, and $A$ is the transport constant. The carrier concentration of the doped $In_2O_3$ thin films clearly changed due to different doping levels. This was observed from the electrical performance results of the Cu-doped $In_2O_3$ thin films. Under a DC power of 20 W, the carrier concentration reached its maximum value, resulting in the smallest overall Seebeck coefficient of the corresponding sample. The carrier concentration was the main factor affecting the variations in the Seebeck coefficients in the temperature range from room temperature to 600 °C. Figure 17 presents the output voltage of the Cu-doped $In_2O_3$ films under 20 W DC power for three heating processes. In the third heating process, the output value reached 89.3 mV at a 600 °C temperature difference; the Seebeck coefficient reached 148.8 μV/°C. The measurement results of the three heating processes indicated that the thermocouple had good repeatability.

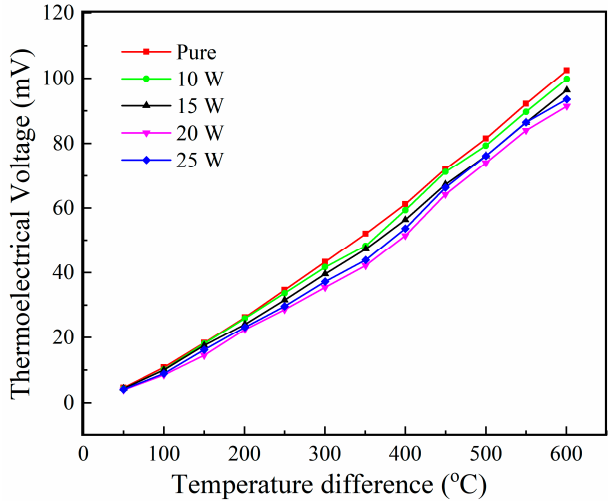


**Figure 15.** Thermoelectrical output voltage of Cu-doped $In_2O_3$/Pt thermocouple under different DC powers.

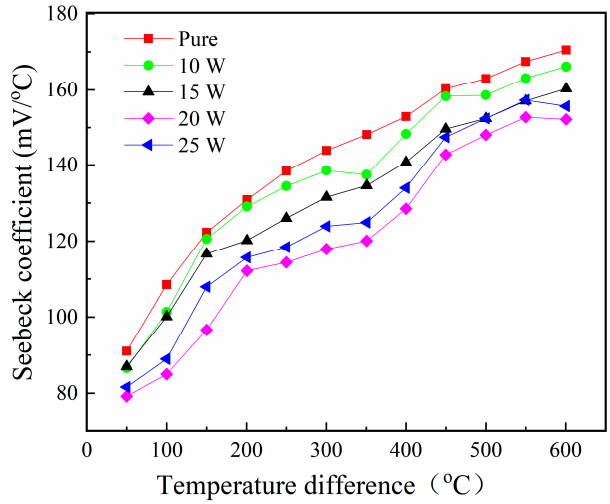


**Figure 16.** Variations in the Seebeck coefficients of a Cu-doped $In_2O_3$/Pt thermocouple under different DC powers.

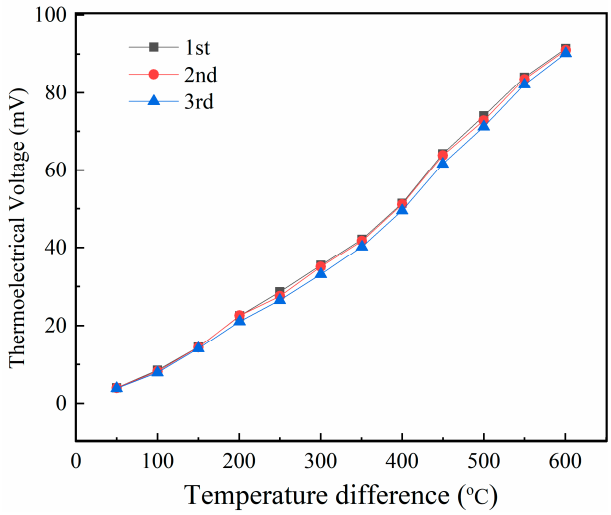


**Figure 17.** Variations in the $In_2O_3$/Pt thermocouple output voltage for three heating processes under 20 W DC power.

## 4. Conclusions

In summary, this paper presents the preparation as well as the morphological, electrical, and optical properties of pure and Cu-doped $In_2O_3$ thin films fabricated using the magnetron co-sputtering process. The doping of copper effectively adjusted the optoelectronic properties of the $In_2O_3$ thin films and significantly impacted the output performance of the thermocouple. When the Cu atomic content increased to 4.09% (under 20 W DC sputtering power), the Cu-doped thin films possessed the highest resistivity ($30.2 \times 10^{-3}$ Ω·cm) and carrier concentration ($3.72 \times 10^{-19}$ $cm^{-3}$) as well as the lowest carrier mobility (0.56 $cm^2V^{-1}s^{-1}$). Copper doping resulted in a significant reduction in the optical band gap. Consequently, the band gap of Cu-doped $In_2O_3$ was narrower than that of undoped $In_2O_3$. The optical band gap was reduced to 2.71 eV when the DC power was 20 W. The Seebeck coefficient of the undoped $In_2O_3$/Pt thermocouple reached a maximum of 170.5 μV/°C and an output value of 106.5 mV at a high-temperature range of 600 °C. When the DC sputtering power was 20 W, the output value of the sample was 91.4 mV and the Seebeck coefficient was 152.1 μV/°C.

**Author Contributions:** Formal analysis, Y.L., T.L., R.H., J.S. and S.C.; investigation, Y.L., T.L. and R.H.; writing, Y.L. and R.H.; writing—review and editing, Y.L., T.L., R.H., J.S. and S.C.; supervision, Y.L., T.L. and R.H. All authors have read and agreed to the published version of the manuscript.

**Funding:** This research was supported by the Shaanxi Provincial Department of Education Youth Innovation Team Project (No. 22JP051).

**Data Availability Statement:** Data are contained within the article.

**Conflicts of Interest:** The authors declare no conflicts of interest.

## References

1. Sakthivel, P.; Murugana, R.; Asaithambi, S.; Karuppaiah, M.; Vijayaprasath, G.; Rajendran, S.; Hayakawa, Y.; Ravi, G. Studies on optoelectronic properties of magnetron Sputtered cadmium stannate ($Cd_2SnO_4$) thin films as alternative TCO materials for solar cell applications. *Ceram. Int.* **2018**, *44*, 2529–2538. [CrossRef]
2. Sakthivel, P.; Murugan, R.; Asaithambi, S. Influence of radiofrequency power on structural, morphological, optical and electrical properties of magnetron sputtered CdO: Sm thin films as alternative TCO for optoelectronic applications. *J. Alloys Compd.* **2018**, *765*, 146–157. [CrossRef]
3. Chan, Y.P.; Seong, P.J.; Joon, B.P. High-performance ITO/a-IGZO heterostructure TFTs enabled by thickness-dependent carrier concentration and band alignment manipulation. *Ceram. Int.* **2023**, *49*, 5905–5914.
4. Sarath, R.; Narasimha, M.Y.; Hari, P.K.; Alshahrani, T.; Sarah, J.M.; Mohd, S.; AlFaify, S. Enhancement in optoelectronic nature of facile spray fabricated Ce co-doped CdO:Zn films for TCO applications. *Optik* **2020**, *223*, 165408.

5. Husam, R.A.; Ameer, I.K.; Ali, A.Y. AImpact of high vacuum annealing temperature on the structural, photoluminescence, and room temperature liquefied petroleum gas sensing of direct current magnetron sputtered CdO films. *Mater. Chem. Phys.* **2022**, *289*, 126446.
6. Liu, Y.T.; Wang, W.X.; Ma, J.P. Structure, optical and electrical properties of Nb-doped ZnO transparent conductive thin films prepared by co-sputtering method. *J. Adv. Dielect.* **2019**, *9*, 1950048. [CrossRef]
7. Daseul, H.; Seongchan, O.; Hyon, C.K. Competing phases in epitaxial $SnO_2$ thin films deposited on sapphire (0001) substrates using radio-frequency powder sputtering. *Ceram. Int.* **2022**, *48*, 28396–28403.
8. Afroz, K.; Rahman, F.; Razia, N.; Asokan, K. Role of deposition temperature and Sn content on structural, optical & electrical properties of $In_2O_3$ thin films. *Curr. Appl. Phys.* **2022**, *38*, 49–58.
9. Vilca-Huayhua, C.A.; Paz-Corrales, K.J.; Aragón, F.F.H.; Mathpalb, M.C.; Villegas, L.L.; Coaquira, J.A.H.; Pacheco-Salazara, D.G. Growth and vacuum post-annealing effect on the structural, electrical and optical properties of Sn-doped $In_2O_3$ thin films. *Thin Solid Film.* **2020**, *709*, 138207. [CrossRef]
10. Ehsan, E.; Fariborz, T. Development of highly sensitive ZnO/$In_2O_3$ composite gas sensor activated by UV-LED. *Sens. Actuators B* **2017**, *241*, 828–839.
11. Nasrin, J.; Mohsen, G.; Vishtasb, S. Investigation of the role of deposition rate on optical, microstructure and ethanol sensing characteristics of nanostructured Sn doped $In_2O_3$ films. *MRS Bull.* **2018**, *106*, 49–56.
12. Rombach, J.; Bierwagen, O.; Papadogianni, A.; Mischob, M.; Cimalla, V.; Berthold, T.; Krischok, S.; Himmerlich, M. Electrical conductivity and gas-sensing properties of Mg-doped and undoped single-crystalline $In_2O_3$ thin films: Bulk vs. Surface. *Procedia Eng.* **2015**, *120*, 79–82. [CrossRef]
13. Pramodn, N.; Pandey, S. Effect of Li doping on the structural, optical and formaldehyde sensing properties of $In_2O_3$ thin films. *Ceram. Int.* **2015**, *41*, 527–532. [CrossRef]
14. Shinozaki, B.; Takada, S.; Kokubo, N. Superconducting characteristics and microstructure of polycrystalline Zn-doped $In_2O_3$ films. *Physica C* **2011**, *471*, 717–720. [CrossRef]
15. Pramodn, N.; Pandey, S. Influence of Sb doping on the structural, optical, electrical and acetonesensing properties of $In_2O_3$ thin films. *Ceram. Int.* **2014**, *40*, 3461–3468. [CrossRef]
16. Moustafa, A.; Ahmed, B.; Essam, R.S. Optical characteristics with high accuracy of diluted Cr doped $In_2O_3$ thin films using spectroscopic ellipsometry for optoelectronic devices. *Opt. Mater.* **2022**, *133*, 113039.
17. Jianhua, S.; Fanying, M.; Jian, B.; Yongwu, L.; Zhengxin, L. Surface scattering effect on the electrical mobility of ultrathin Ce doped $In_2O_3$ film prepared at low temperature. *Mater. Lett.* **2018**, *225*, 54–56.
18. Wang, G.H.; Shi, C.Y.; Zhao, L. Efficiency improvement of the heterojunction solar cell using an antireflection Hf-doped $In_2O_3$ thin film prepared via glancing angle magnetron sputtering technology. *Opt. Mater.* **2020**, *109*, 110323. [CrossRef]
19. Chaeyoung, K.; Hae, J.S.; Seong, W.K. Ga and Ti co-doped $In_2O_3$ films for flexible amorphous transparent conducting oxides. *Ceram. Int.* **2022**, *48*, 13938–13947.
20. Kaleemulla, S.; Rao, N.M. Electrical and optical properties of $In_2O_3$:Mo thin films prepared at various Mo-doping levels. *J. Alloys Compd.* **2010**, *504*, 351–356. [CrossRef]
21. Fan, Y.; Xing, M.C.; Xue, Z.; Tian, X.Q. The electrical and optical properties of Cu-doped $In_2O_3$ thin films. *Thin Solid Film.* **2014**, *556*, 44–47.
22. Gregory, O.J.; Tougas, I.M.; Amani, M.; Crisman, E.E. Thermoelectric Properties and Microstructure of Cu-In-O Thin Films. *ACS Comb. Sci.* **2013**, *15*, 580–584. [CrossRef] [PubMed]
23. Gupta, R.K.; Ghosh, K.; Mishra, S.R.; Kahol, P.K. High mobility, transparent, conducting Gd-doped $In_2O_3$ thin films by pulsed laser deposition. *Thin Solid Film.* **2008**, *516*, 3204–3209. [CrossRef]
24. Salvador, A.; Palomares, S.; Bernard, E. Sol-gel growth and characterization of $In_2O_3$ thin films. *Thin Solid Film.* **2018**, *645*, 383–390.
25. Baqiah, H.; Ibrahim, N.B. Electrical transport, microstructure and optical properties of Cr-doped $In_2O_3$ thin film prepared by sol-gel method. *J. Alloys Compd.* **2013**, *575*, 198–206. [CrossRef]
26. Xuejian, D.; Jing, Y.; Xianwu, X.; Qianqian, S.; Wei, T.; Baoyuan, M. Epitaxial growth and characterization of high quality $In_2O_3$ films on a-plane sapphire substrates by MOCVD. *Vacuum* **2019**, *167*, 1–5.
27. Shinho, C. Effects of rapid thermal annealing on the properties of $In_2O_3$ thin films grown on glass substrate by rf reactive magnetron sputtering. *Microelectron. Eng.* **2012**, *89*, 84–88.
28. Zijian, Y.; Xiaming, Z.; Xiong, W.; Xikun, C.; Bingpo, Z.; Dongjiang, Q.; Huizhen, W. Annealing effects of $In_2O_3$ thin films on electrical properties and application in thin film transistors. *Thin Solid Film.* **2011**, *519*, 3254–3258.
29. Otto, J.G.; Qing, L.; Everett, E.C. High temperature stability of indium tin oxide thin films. *Thin Solid Film.* **2002**, *406*, 286–293.
30. Dyer, S.E.; Gregory, O.J.; Amons, P.S.; Slot, B.A. Preparation and piezoresistive properties of reactively sputtered indium tin oxide thin films. *Thin Solid Film.* **1996**, *288*, 279–286. [CrossRef]
31. Zhao, X.H.; Li, H.T.; Jiang, S.W.; Zhang, W.L.; Jiang, H.C. Effect of nitrogen doping on the thermoelectric properties of ITO-$In_2O_3$ thin film thermocouples. *Thin Solid Film.* **2017**, *629*, 1–5. [CrossRef]
32. Liu, D.; Shi, P.; Ren, W. Fabrication and characterization of $La_{0.8}Sr_{0.2}CrO_3$/$In_2O_3$ thin film thermocouple for high temperature sensing. *Sens. Actuators A* **2018**, *280*, 459–465. [CrossRef]
33. Zhao, X.H.; Li, H.T.; Chen, Y.Z.; Jiang, H.C. Preparation and thermoelectric characteristics of ITO/Pt thin film thermocouples on Ni-based superalloy substrate. *Vacuum* **2017**, *140*, 116–120. [CrossRef]

34. Zhang, Z.K.; Tian, B.; Li, L.; Lei, J.M.; Liu, Z.J.; Liu, J.J.; Cheng, G.; Zhao, N.; Fang, X.B.; Zhao, L.B. The electrical and optical properties of Cu-doped $In_2O_3$ thin films. *Ceram. Int.* **2022**, *48*, 25747–25755. [CrossRef]
35. Zhao, X.H.; Li, H.T.; Yang, K.; Jiang, S.W.; Jiang, H.C.; Zhang, W.L. Annealing effects in ITO based ceramic thin film thermocouples. *J. Alloys Compd.* **2017**, *698*, 147–151. [CrossRef]
36. Liu, Y.T.; Ren, W.; Shi, P.; Liu, D. Preparation and thermal volatility characteristics of $In_2O_3$/ITO thin film thermocouple by RF magnetron sputtering. *AIP Adv.* **2017**, *7*, 1150251–1150258. [CrossRef]
37. Jingli, S.; Feng, L.; Bo, Y.; Liang, S.; Chuan, C.; Shanpeng, W.; Yu, C.; Shengping, R. Enhanced ethyl acetate sensing performance of Al-doped $In_2O_3$ microcubes. *Sens. Actuators B* **2017**, *253*, 461–469.
38. Asma, A.; Azra, P. Tuning the structural, optical, and magnetic properties of $In_2O_3$ nanoparticles with an evaluation of its antibacterial efficiency via controlling the doping concentrations of Ni, Co, and Fe. *Mater. Today Commun.* **2022**, *30*, 103063.
39. Shanmuga, P.B.; Shanthi, M.; Manoharan, C.; Bououdina, M. Hydrothermal synthesis of Ga-doped $In_2O_3$ nanostructure and its structural, optical and photocatalytic properties. *Mater. Sci. Semicond. Process.* **2017**, *71*, 357–365. [CrossRef]
40. Mengting, L.; Qiuqiang, Z.; Wei, L.; Rui, L.; Qinyu, H.; Yinzhen, W. Effect of Zn doping concentration on optical band gap of PbS thin films. *J. Alloys Compd.* **2019**, *792*, 1000–1007.
41. Miao, W.; Li, X.; Zhang, Q. Transparent conductive $In_2O_3$:Mo thin films prepared by reactive direct current magnetron sputtering at room temperature. *Thin Solid Film.* **2006**, *500*, 70–73. [CrossRef]
42. Fernando, P.S.; Su, H.W.; Anderson, J. Enabling visible-light absorption and p-type doping in $In_2O_3$ by adding Bi. *Phys. Rev. Mater.* **2019**, *3*, 034605.
43. Nasser, Y.M.; Ali, B.; Sameh, I.A. Influence of Cu and Ag doping on structure and optical properties of $In_2O_3$ thin film prepared by spray pyrolysis. *Results Phys.* **2018**, *10*, 126–131.
44. Ian, M.T.; Matin, A.; Otto, J.G. Metallic and Ceramic Thin Film Thermocouples for Gas Turbine Engines. *Sensors* **2013**, *13*, 15324–15347.
45. Liu, Y.T.; Ren, W.; Shi, P.; Liu, D. Highly Thermostable $In_2O_3$/ITO Thin Film Thermocouple Prepared via Screen Printing for High Temperature Measurements. *Sensors* **2018**, *18*, 958. [CrossRef]